Internal Electric Field and Second Harmonic Generation in the Blends of Vinylidene Fluoride–Trifluoroethylene Copolymer and Poly(methyl methacrylate) with a Pendant Nonlinear Optical Dye

Naoto Tsutsumi,* Tsuyoshi Ono, and Tsuyoshi Kiyotsukuri

Department of Polymer Science & Engineering, Kyoto Institute of Technology, Matsugasaki, Sakyoku, Kyoto 606, Japan

Received April 1, 1993; Revised Manuscript Received June 16, 1993•

ABSTRACT: This paper presents the internal electric field created by the preferentially oriented β-crystallite dipoles in the blends of 75 mol % vinylidene fluoride–25 mol % trifluoroethylene copolymer (P(VDF-TrFE)) and poly(methyl methacrylate) (PMMA) and the second harmonic generation (SHG) from the oriented β-crystallite dipoles and that from the nonlinear optical (NLO) dyes noncentrosymmetrically aligned by the internal electric field. We have also prepared the copolymer of methyl methacrylate (MMA) with a vinyl monomer having a NLO pendant amino–nitro–azobenzene (P(MMA-*co*-MMA-DR1)) as a SHG active polymer. The blends of both P(VDF-TrFE)/PMMA and P(VDF-TrFE)/P(MMA-*co*-MMA-DR1) with low DR1 content (experimentally up to 4 mol %) show optical clarity that is desirable for SHG materials. Internal electric fields (E_i) of 1.7–3.2 MV/cm, which is significantly larger than the applied field of 0.8 MV/cm, were measured at the P(VDF-TrFE) content above 70 mol %. SHG coefficient d_{33} values are 3.3×10^{-9}, 2.3×10^{-9}, and 0.9×10^{-9} esu for P(VDF-TrFE), (90/10) P(VDF-TrFE)/PMMA, and (90/10) P(VDF-TrFE)/P(MMA-*co*-MMA-DR1), respectively. Temperature profiles of E_i for the blends are shared by those of pyroelectricity and those of d_{33}. Their activities are not significantly depressed at the glass transition temperature T_g but are drastically lost at the temperature around the Curie transition temperature, which is higher than T_g. We will discuss the nature of the thermal stability of the internal electric field, pyroelectricity, and SHG activity, relating to the order–disorder transition of β-crystallite dipoles at the Curie transition temperature.

Introduction

Polymeric materials having a second harmonic generation (SHG) must be macroscopically noncentrosymmetric. For these materials, electrical poling is a common procedure to break a center of symmetry of randomly oriented nonlinear optical (NLO) dye molecules to achieve noncentrosymmetric alignment. However, the preferential alignment of NLO molecules was perturbed or disoriented by a molecular relaxation of materials, even if the sample was kept at temperatures below the glass transition temperature (T_g). Many efforts have been made to suppress the relaxation of NLO molecules in the polymeric matrix.[1-3]

Hill et al.[4] demonstrated that the internal electric field (E_i) created by the preferentially oriented polar crystals of the copolymer of vinylidene fluoride and trifluoroethylene (P(VDF-TrFE)) can orient polar molecules which dissolve in the amorphous region of the copolymer. Using guest molecules which have NLO properties, they showed that such poled copolymer films exhibit a SHG arising from the oriented NLO molecules.

Tsutsumi et al.[5] have also studied E_i created by the aligned β-crystallite dipoles of the P(VDF-TrFE) copolymer using the electrochromic spectrum shift of dye dissolved in the copolymer and discussed the correlation between E_i and remanent polarization as well as the thermal stability of E_i. In their article, E_i was stable and almost constant until its sudden decrease occurred near the Curie transition temperature, which was shared by the thermal stability of pyroelectricity.

P(VDF-TrFE) copolymer has large light scattering in the UV–visible region due to the presence of small crystallites or the spherulite developed in the semicrystalline polymer. However, the blend of P(VDF-TrFE) and poly(methyl methacrylate) (PMMA) has low light scattering property, even when it has a β-crystalline phase. These results will allow this blend to be a candidate for a SHG material. The miscibility of the blends of P(VDF-TrFE) and PMMA has been studied, and it was found that P(VDF-TrFE) and PMMA form compatible blends,[6] as in the case of the blends of poly(vinylidene fluoride) (PVDF) and PMMA.[7]

In this paper, we have investigated E_i, the pyroelectric coefficient (C_{pyro}), and SHG activity in P(VDF-TrFE)/PMMA blends, as well as their thermal stabilities. E_i created by the aligned β-crystallite dipoles in P(VDF-TrFE)/PMMA blends is measured by the spectrum shift of dye molecule dispersed in the blends, as was done previously for P(VDF-TrFE).[5] Furthermore, we have synthesized the copolymer of methyl methacrylate (MMA) with a vinyl monomer having a pendant amino–nitro–azobenzene group (P(MMA-*co*-MMA-DR1)) as a NLO active polymer. The thermal stability of SHG activity for the blend of P(VDF-TrFE) with P(MMA-*co*-MMA-DR1) has also been investigated.

Experimental Section

Sample Preparation. 4-(Dimethylamino)-4′-nitrostilbene (DANS) from Eastman Kodak Co., as an electrochromic probe for measuring the internal electric field, was recrystallized from amyl alcohol. The copolymer of 75 mol % vinylidene fluoride and 25 mol % trifluoroethylene (P(VDF-TrFE)) was supplied by Atochem and used as received. PMMA from Sumitomo Chemical Co. was reprecipitated in methanol from acetone solution.

Scheme I shows the procedure for making a P(MMA-*co*-MMA-DR1) copolymer containing 4-[ethyl(2-hydroxyethyl)amino]-4′-nitroazobenzene (Disperse Red, 1, DR1) as a pendant NLO group. DR1 obtained from Aldrich Chemical Co. was used as received. DR1 was reacted with methacryloyl chloride in methylene chloride in the presence of ethanolamine at 0 °C for 2 h in nitrogen atmosphere and additionally at room temperature for 2 h to obtain DR1 vinyl monomer. A mixture of DR1 vinyl monomer and MMA of a given molar ratio was copolymerized with AIBN as

* To whom all correspondence should be addressed.

• Abstract published in *Advance ACS Abstracts*, September 1, 1993.

0024-9297/93/2226-5447$04.00/0

Scheme I

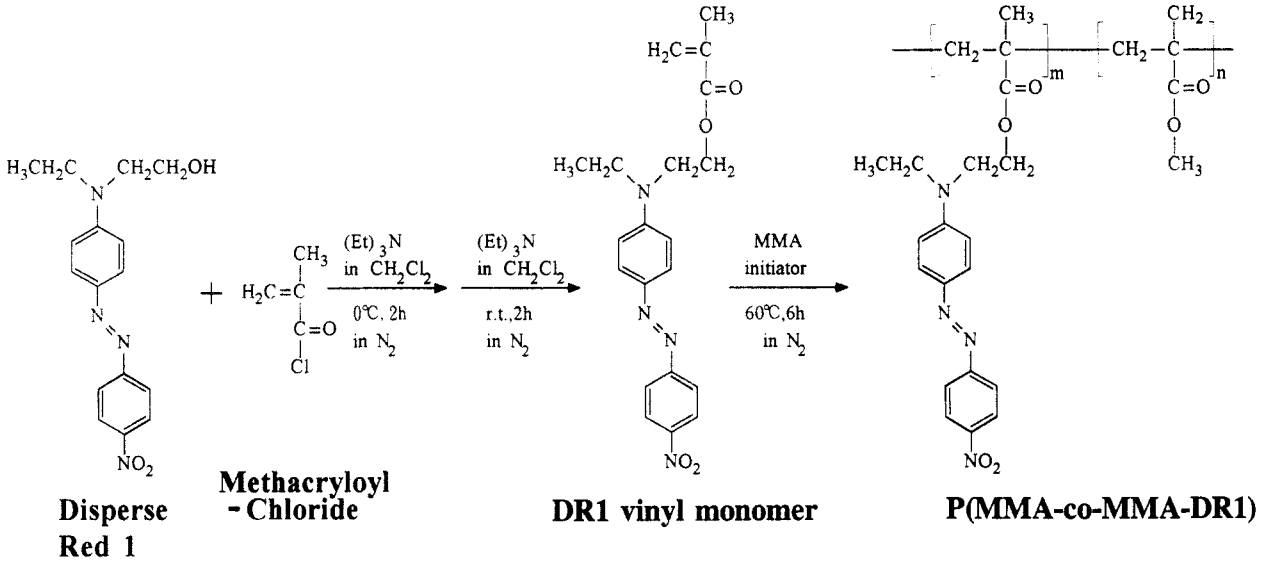

an initiator at 60 °C for 6 h in nitrogen atmosphere to obtain P(MMA-*co*-MMA-DR1). Then the obtained product was reprecipitated in methanol from acetone solution. The content of DR1 vinyl monomer unit in P(MMA-*co*-MMA-DR1) was determined by an elemental analysis. P(MMA-*co*-MMA-DR1) polymers with 1, 4, 8, and 14 mol % DR1 vinyl monomer unit were obtained and referred to as P(MMA-*co*-MMA-DR1-1), P(MMA-*co*-MMA-DR1-4), P(MMA-*co*-MMA-DR1-8), and P(MMA-*co*-MMA-DR1-14), respectively.

P(VDF-TrFE) and PMMA were dissolved in acetone containing DANS of 2×10^{-2} mol/L and cast on a substrate to obtain DANS containing P(VDF-TrFE)/PMMA blends. Blend films were melt-pressed at 200 °C between 150-μm-thick Upilex polyimide films on a heated press to a thickness of 40–100 μm. The molten films were quenched into liquid nitrogen. P(VDF-TrFE)/P(MMA-*co*-MMA-DR1) blend films were also prepared in a similar manner.

Blend films were annealed at 100 °C for 30 min, and aluminum electrodes were deposited onto opposing film surfaces prior to poling. P(VDF-TrFE) and P(VDF-TrFE)/PMMA (99/1 by weight) were poled in a Fluorinert at room temperature for 1 h, and P(VDF-TrFE)/PMMA with other blend ratios and P(VDF-TrFE)/P(MMA-*co*-MMA-DR1) blends were poled in an oven at 80–100 °C for 0.5–1 h.

Electrical and Optical Measurements. C_{pyro} was determined by measuring the current generated upon heating and cooling the poled film at a measured rate of 1–2 °C/min in the vicinity of 25–30 °C. After the pyroelectric response was measured, the aluminum electrodes were removed by immersing in 0.1 N NaOH for a few minutes in order to make the subsequent optical measurements. Ultraviolet–visible spectra of the films were measured on a Shimadzu Model UV-2101PC spectrophotometer controlled by a micro-PC and a Perkin-Elmer Model Lamda 9 PC microcomputer-controlled UV–vis–near IR spectrophotometer equipped with an integrating sphere. The measured spectra were obtained in transmission and were stored by 0.5-nm intervals in a microcomputer for analysis. As in prior work on P(VDF-TrFE) copolymer[5] and the blend of PVDF and PMMA,[8,9] we deduced E_i created by the aligned β-crystallite dipoles from the spectrum shift and broadening of the DANS probe.

Refractive indices of the films were measured using an Atago Abbe refractometer Model 1T with monochromated light through an interference filter at 470, 530, 610, 660, and 1060 nm. When a refractive index was measured at 1060 nm, a near infrared viewer was used to convert near infrared light to visual.

The SHG was measured by the Maker fringe method[10,11] whose schematic diagram is shown in Figure 1. The laser source was a Continuum Model Surelite-10 Q-switched Nd:YAG pulse laser with a 1064-nm p-polarized fundamental beam, 320-mJ maximum energy, 7-ns pulse width, and 10-Hz repeating rate. The laser beam reflected from a glass surface was incident upon an attenuator consisting of a λ/2 waveplate and a plate polarizer and then upon a 10% transmission neutral density filter for the Nd:YAG laser. The laser energy was monitored with a Molectron J25LP low profile pyroelectric joulemeter equipped with a Model JD501 joulemeter digitizer. The obtained laser power was transferred from a digitizer to a microcomputer through a Stanford Research Systems (SRS) SR-245 interface module. The laser power illuminated to the sample film was ca. 0.2 mJ. The plate polarizer in an attenuator also improved the p-polarized beam quality. If an s-polarized laser beam was needed, the λ/2 waveplate (polarizer in Figure 1) was used to convert the p-polarized to an s-polarized beam. The p- or s-polarized laser beam passed through an IR pass filter (a UV–visible light cut filter) was focused on the sample film on a rotating stage equipped with a heater, a thermocouple, and a microcomputer-controlled stepping motor. The second harmonic (SH) wave generated through two pieces of IR cut filters, a third harmonic generation cut filter, an interference filter at 532 nm, a neutral density filter if necessary, and an analyzer was detected by a Hamamatsu Model R928 photomultiplier. The SH signal averaged on a SRS Model SR-250 gated integrator and boxcar averager module was transferred to a microcomputer through a SRS Model SR-245 computer interface module. The gated pulse signal and SH pulse signal were directly monitored on a Lecroy Model 9310 300-MHz digital oscilloscope. The delay time on the SR-250 was adjusted so that the SH pulse signal was within the 12-ns gate pulse. A λ/2 waveplate in an attenuator, another λ/2 waveplate for a polarizer, and an analyzer were also individually rotated by microcomputer-controlled stepping motors.

Thermal pulse measurement was done using a ruby laser modified to produce a pulse duration of nominally 100-ns half-width at half-maximum. The thermal pulse method and the analytical methods used to interpret thermal pulse data are discussed elsewhere.[12,13] The pulse duration is much smaller than the thermal equilibration time of the samples, which is of the order of 1 ms. The information of interest in this paper is derived from the thermal pulse response signals without determining the shape of the polarization distribution by numerical deconvolution of these signals. The signals presented here are ten-shot summation averages of the charge flowing from one electrode to the other around an external circuit as a function of time following the application of a thermal pulse to one surface. Signals are presented in pairs, one obtained by applying thermal pulses to one surface, the other signal obtained by applying thermal pulses to the opposite surface.

Characterization. Differential thermal analysis (DTA) was carried out using a Shimadzu DT-30 differential thermal analyzer at a heating rate of 10 °C/min in a nitrogen atmosphere. Thermomechanical analysis (TMA) was performed in a penetration mode under a pressure of 10 kg/cm² and a heating rate of 10 °C/min in a nitrogen atmosphere, using a Seiko Instruments Model TMA 100 thermomechanical analyzer controlled by a SSC-

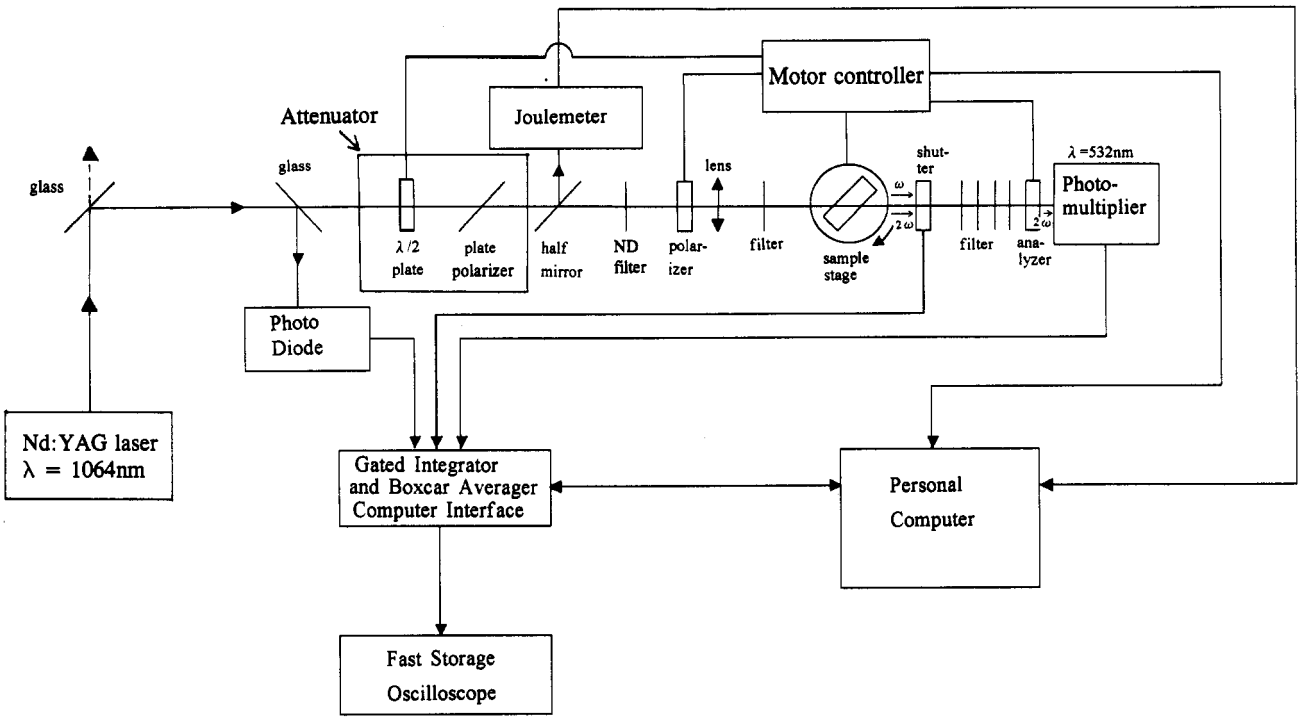

Figure 1. Schematic diagram of the Maker fringe measurement.

5200 disk station. Wide angle X-ray scattering (WAXS) patterns of the films were measured with a Toshiba Model ADG-301 X-ray diffractometer with nickel-filtered Cu Kα radiation, and the obtained patterns were transferred to a microcomputer for data analysis.

Basis for Measurement of the Internal Electric Field

A theory for electrochromic effects in liquid solutions was developed and published by Liptay and co-workers in a series of papers which are well summarized in ref 14. The theory was applied to electrochromic molecules dissolved in a polymer matrix by Havinga and van Pelt.[15] Stated simply, optical absorption corresponds to energy transfer between an electronic ground and an electronic excited state in a molecule. In the presence of an electric field, the energy of each state is reduced by the product of the dipole moment μ, the field E, and the cosine of the angle between the dipole and the field. The energy difference between the ground and the excited states at a particular angular position is then altered by an amount proportional to the electric field and the difference in dipole moment between the two states. The angular distribution of dipoles with respect to the field is estimated from the Langevin function in terms of the dimensionless variable $\mu E/(kT)$. Molecular parameters which enter the theory are the dipole moments of the ground state μ_g and the excited state μ_e and the angles between the dipole moments and a coordinate system within the molecule. For large values of μ, terms involving the polarizations of the two states are negligible.

The absorption spectra of the probe molecules are rather broad and the shifts in the peak maxima are small so that spectral shifts are best determined by comparing large portions of the two spectra. For this purpose, it has been found convenient to express the spectrum in the presence of a field $A(\nu,E)$ as a Taylor series expansion of the unperturbed spectrum $A(\nu,0)$ with the wavenumber shift $\Delta\nu$ as the perturbation. Furthermore, according to Liptay,[14] the absorption spectrum is practically identical to a Lorentzian line shape if expressed as absorbance divided by wavenumber. Following Havinga and van Pelt,[15]

$$\frac{A(\nu,E)}{\nu} - \frac{A(\nu,0)}{\nu} = \delta\frac{A(\nu,0)}{\nu} + \langle\Delta\nu\rangle\frac{\partial}{\partial\nu}\frac{A(\nu,0)}{\nu} + \frac{1}{2}\langle(\Delta\nu)^2\rangle\frac{\partial^2}{\partial\nu^2}\frac{A(\nu,0)}{\nu} \quad (1)$$

The term involving δ accounts for a change in absorbance due to reorientation of the dye in the presence of the field. Terms involving $\langle\Delta\nu\rangle$ and $\langle(\Delta\nu)^2\rangle$ describe field-induced shifts in the band and field-induced broadening of the band,[15] respectively. The decrease of absorption intensity by poling is not only due to the reorientation (alignment) of DANS to the internal field but also to the loss of some DANS when the sample is poled at 80 °C and annealed at high temperatures up to 130 °C. If we assume that the intensity of the absorbance is reduced uniformly by a factor f across all wavelengths in the absorption band and neglect terms above $\langle(\Delta\nu)^2\rangle$, the poled spectrum can be expressed in terms of the unpoled spectrum by

$$\frac{1}{(1-f)}\frac{A(\nu,E)}{\nu} - \frac{A(\nu,0)}{\nu} = \delta\frac{A(\nu,0)}{\nu} + \langle\Delta\nu\rangle\frac{\partial}{\partial\nu}\frac{A(\nu,0)}{\mathrm{n}} + \frac{1}{2}\langle(\Delta\nu)^2\rangle\frac{\partial^2}{\partial\nu^2}\frac{A(\nu,0)}{\nu} \quad (2)$$

The theoretical expressions for δ, $\langle\Delta\nu\rangle$, and $\langle(\Delta\nu)^2\rangle$ in the paper of Havinga and van Pelt[15] can be modified[5] to simplified forms of

$$\delta = -G(u) \quad (3)$$

$$\langle\Delta\nu\rangle = -\frac{G(u)}{1-G(u)}3C \quad (4)$$

$$\langle(\Delta\nu)^2\rangle = \frac{G(u)}{1-G(u)}3C^2 \quad (5)$$

$$G(u) = 1 - \frac{3\coth(u)}{u} + \frac{3}{u^2} \quad (6)$$

$$u = \frac{E_i\mu_g}{kT} \quad (7)$$

$$C = \frac{kT\Delta\mu}{hc\mu_g} \tag{8}$$

where k is Boltzmann's constant, T is the absolute temperature, $\Delta\mu$ is the difference between the dipole moments in the excited state and in the ground state ($=\mu_g - \mu_e$), h is Planck's constant, and c is the speed of light. Substitution of the expressions for δ, $\langle\Delta\nu\rangle$, and $\langle(\Delta\nu)^2\rangle$ in eq 2 by eqs 3–5, respectively and the subsequent rearranging result in the final equation of

$$\frac{1}{(1-f)(1-G(u))}\frac{A(\nu,E)}{\nu} - \frac{A(\nu,0)}{\nu} = \frac{G(u)}{(1-G(u))^2}\left[-3C\frac{\partial}{\partial\nu}\frac{A(\nu,0)}{\nu} + \frac{3}{2}C^2\frac{\partial}{\partial\nu^2}\frac{A(\nu,0)}{\nu}\right] \tag{9}$$

Details of internal electric field calculation will appear in a section of the Results and Discussion.

Second Harmonic Generation

The second harmonic coefficients of the sample films were determined by the Maker fringe analysis.[10,11,16] These measurements were made relative to a Y-cut quartz plate ($d_{11} = 1.2 \times 10^{-9}$ esu). In this technique, a plane sample was rotated in the path of a fundamental beam of wavelength 1064 nm from a Q-switched Nd:YAG pulse laser. The second harmonic power $P_{2\omega}$ detected is given by

$$P_{2\omega} = \frac{512\pi^3}{A}t_\omega^4 T_{2\omega}\frac{d^2p^2(\theta)}{(n_\omega^2 - n_{2\omega}^2)^2}P_\omega^2 \sin^2\Psi \tag{10}$$

where A is the beam area, t_ω and $T_{2\omega}$ are the transmission factors for the incident fundamental and the second harmonic light, respectively, n_ω and $n_{2\omega}$ are the refractive indices of the incident fundamental and the second harmonic light, respectively, d is the second harmonic coefficient, $p(\theta)$ is the projection factor, and P_ω is the incident fundamental laser power.

$$\Psi = \frac{\pi l}{2}\frac{4}{\lambda}(n_\omega\cos\theta_\omega - n_{2\omega}\cos\theta_{2\omega}) \tag{11}$$

where l is the film thickness, λ is the wavelength of the fundamental laser beam, and

$$\sin\theta_\omega = \sin\theta/n_\omega \qquad \sin\theta_{2\omega} = \sin\theta/_{n2\omega} \tag{12}$$

from Snell's law.

Transmission factors are defined as

$$t_\omega = \frac{2\cos\theta}{n_\omega\cos\theta + \cos\theta_\omega} \tag{13}$$

for the p-polarized fundamental light,

$$t_\omega = \frac{2\cos\theta}{n_\omega\cos\theta_\omega + \cos\theta} \tag{14}$$

for the s-polarized fundamental light, and

$$T_{2\omega} = 2n_{2\omega}\cos\theta_{2\omega}\frac{(n_\omega\cos\theta + \cos\theta_\omega)(n_{2\omega}\cos\theta_\omega + n_\omega\cos\theta_{2\omega})}{(n_{2\omega}\cos\theta_{2\omega} + \cos\theta)^3} \tag{15}$$

for the p-polarized second harmonic light.

Projection factors are defined as

$$dp(\theta) = d_{33}\left[\left(\sin^2\theta_\omega + \frac{1}{3}\cos^2\theta_\omega\right)\sin\theta_{2\omega} + \frac{2}{3}\cos\theta_\omega\sin\theta_\omega\cos\theta_{2\omega}\right] \tag{16}$$

for the p-polarized fundamental and p-polarized second harmonic light and

$$dp(\theta) = 2d_{31}\sin\theta_\omega\cos\theta_\omega\cos\theta_{2\omega} \tag{17}$$

for the s-polarized fundamental and p-polarized second harmonic light.

Coherence length l_c ($=\lambda/[4|n_\omega - n_{2\omega}|]$) is calculated using refractive indices measured at 530 and 1060 nm.

Results and Discussion

Polymer Structure. Figures 2 and 3 show DTA curves for P(VDF-TrFE)/PMMA and P(VDF-TrFE)/P(MMA-*co*-MMA-DR1-1), respectively. Melt-quenched PMMA and P(MMA-*co*-MMA-DR1-1) neat samples have T_g at 110 °C. For both systems, T_g decreases with increasing P(VDF-TrFE) content, which implies these polymer blends are miscible in the amorphous region. Melt-quenched P(VDF-TrFE) has a Curie transition temperature (T_c) at 105 °C and a melting point (T_m) at 140 °C. Annealing at 100 °C for 30 min causes sharpening of the endotherm peak of T_c and the slight shift of T_m from 140 to 144 °C. It is noted that T_c for the melt-quenched sample decreases with increasing PMMA content but that for the annealed one is unchanged and appeared at a temperature around 105 °C. T_c is the transition temperature at which the ferroelectric phase changes to the paraelectric phase. The lower T_c may be ascribed to the fact that the ordered ferroelectric phase has not been well developed in the melt-quenched blends. The annealing causes the development of an ordered ferroelectric phase in the blends. T_m and its peak intensity decrease with increasing PMMA content. These decreases imply that the PMMA component works as an inhibitor of β-crystal growth.

Figures 4 and 5 show WAXS results (2θ-scan) for P(VDF-TrFE)/PMMA and P(VDF-TrFE)/P(MMA-*co*-MMA-DR1-1), respectively. The 2θ-scan of P(VDF-TrFE) shows the typical peaks of the β-crystal form at 2θ = 19.8, 35.2, and 40.8°. For the polymer blend whose P(VDF-TrFE) content was 90, 80, and 70 wt %, the peaks at 2θ = 19.8° due to (110)(200) reflection from the β-crystal form[17] that are already perceptible in the melt-quenched blend scan, intensify with annealing at 100 °C for 30 min. These WAXS results are consistent with the results of T_c and T_m mentioned above.

Absorption Spectra. Visually, the blend films were found to be optically clear in the melt-quenched state and after annealing at 100 °C for 30 min. Figure 6a shows absorption spectra for P(VDF-TrFE), (80/20 by weight) P(VDF-TrFE)/PMMA, and DANS containing the (80/20) P(VDF-TrFE)/PMMA blend. The P(VDF-TrFE)/PMMA blend exhibits low light scattering in the ultraviolet and visible regions, whereas an apparent increase in absorbance with decreasing wavelength for the P(VDF-TrFE) film is due to scattering loss caused by the spherulite developed in the semicrystalline polymer.

The effect of poling on the absorption spectrum of DANS is shown in Figure 6b. Poling causes a small shift of the spectral peak at 440 nm to longer wavelength. This shift is ascribed to the change of the electronic state in DANS due to the development of an internal electric field. The intensity drop of the spectrum peak induced by poling is due to the decrease of coupling of the DANS transition

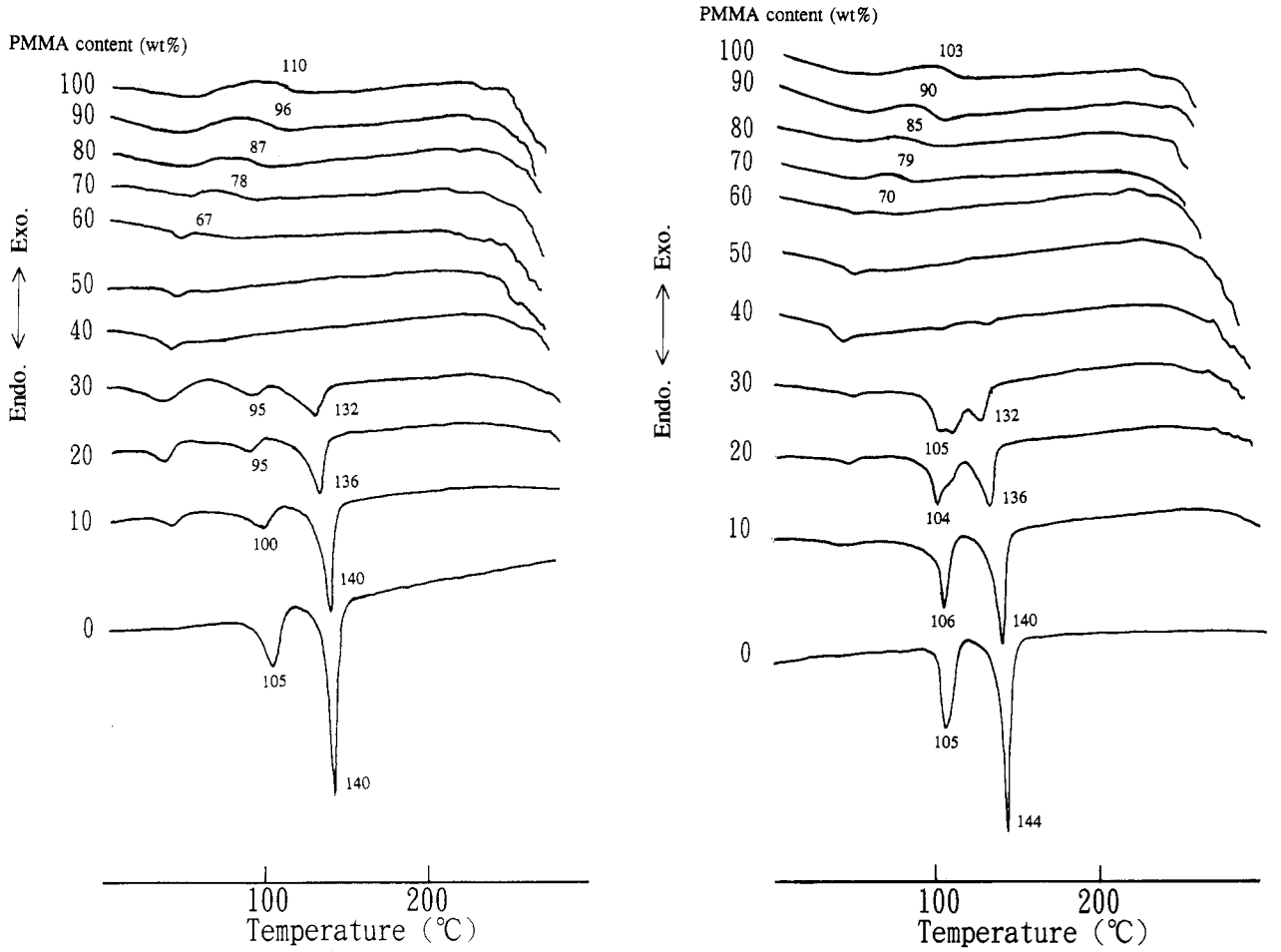

Figure 2. Temperature profiles of DTA scanning of P(VDF-TrFE)/PMMA for various PMMA contents at intervals of 10 wt %: (a, left) melt-quenched samples; (b, right) samples annealed at 100 °C for 30 min.

moment vector with the electric vector of the probing light, which is expected when the DANS dipoles whose vector is parallel to the transition moment vector become aligned with respect to the poling field, and to concentration loss of DANS by sublimation when poled at 80 °C and annealed at temperature up to 130 °C, as mentioned previously. The decrease of intensity thus is not a direct measure of the internal electric field.

Calculation of the Internal Electric Field. The difference in the absorbances divided by ν at several values of ν before and after poling would be fit to the original spectrum and the first and second derivatives of the original curves at the corresponding wavenumbers according to eq 1. Coefficients obtained from such a fit are the orientation-induced change in absorbance δ, the shift in absorption spectra $\langle\Delta\nu\rangle$, and the broadening of the peak $\langle(\Delta\nu)^2\rangle$. However, as mentioned above, changes in absorbances are also caused by a decrease in the concentration of dye. We have introduced the theoretical expression including factor f of eq 2 and arrived at eq 9 involving the electric field, dipole moment, etc., of eqs 3–5.

The spectrum after poling, reduced from the original by factors f and $G(u)$, shifted by $\Delta\nu$, and broadened by $\langle(\Delta\nu)^2\rangle/2$, will cross the original spectrum at some value of wavenumber ν_N, where $A(\nu_N,E)/[(1-f)\{1-G(u)\}\nu_N] = A(\nu_N,0)/\nu_N$. At the intersection, the right-hand side of eq 9 will be equal to zero, from which it can be deduced that $\partial\{A(\nu,0)/\nu\}/\partial\nu = (C/2)\partial^2\{A(\nu,0)/\nu\}/\partial\nu^2$. First and second derivatives of $A(\nu,0)/\nu$ are evaluated as a function of ν to determine the value ν_N for which the above relation was satisfied. A value of $(1-f)\{1-G(u)\}$ was then chosen to make the spectra of the poled and unpoled samples intersect at ν_N, i.e. $A(\nu_N,E)/[(1-f\{1-G(u)\}\nu_N] = A(\nu_N,0)/\nu_N$. Once the curves is normalized at ν_N, the differences in absorbance between the two spectra at several other values of ν are then determined, the derivatives are evaluated at the corresponding values of ν as required for eq 9, and the quantity $[G(u)/\{1-G(u)\}^2]$ is evaluated from a linear least squares fit. From $G(u)$ and eq 6, a value of u is obtained from which E_i is evaluated. The more detailed numerical treatments are described in ref 5.

Internal Electric Field and Pyroelectricity. Figure 7 shows the change of E_i and C_{pyro} for P(VDF-TrFE)/PMMA blends for various PMMA contents by 10 wt % intervals. A sample film was annealed at 100 °C for 30 min prior to poling and then poled at a constant field of 0.8 MV/cm at 80 °C for 30 min and cooled to room temperature for 30 min under the same field. E_i data for the P(VDF-TrFE) neat sample obtained from ref 5 were plotted in Figure 7. Both E_i and C_{pyro} decrease with increasing PMMA content up to 50 wt % and at PMMA contents above 50 wt % almost level off except for the significant incrase of E_i for the PMMA neat sample. E_i values at P(VDF-TrFE) contents above 70 wt % are between 1.7 and 3.2 MV/cm, which is larger than the applied field of 0.8 MV/cm, as is the case for another ferroelectric host.[5,8,9] In the range of PMMA contents between 50 and 90 wt %, the calculated E_i is approximately the same as the poling field of 0.8 MV/cm. The WAXS pattern for the annealed sample shown in Figure 4b was separated into a Lorentzian waveform using a stabilized Gauss–Newton method. The crystallite size of the β-crystal was estimated from the half-width at $2\theta = 19.8°$ due to the (110)(200) reflection, using a Scherrer relation.

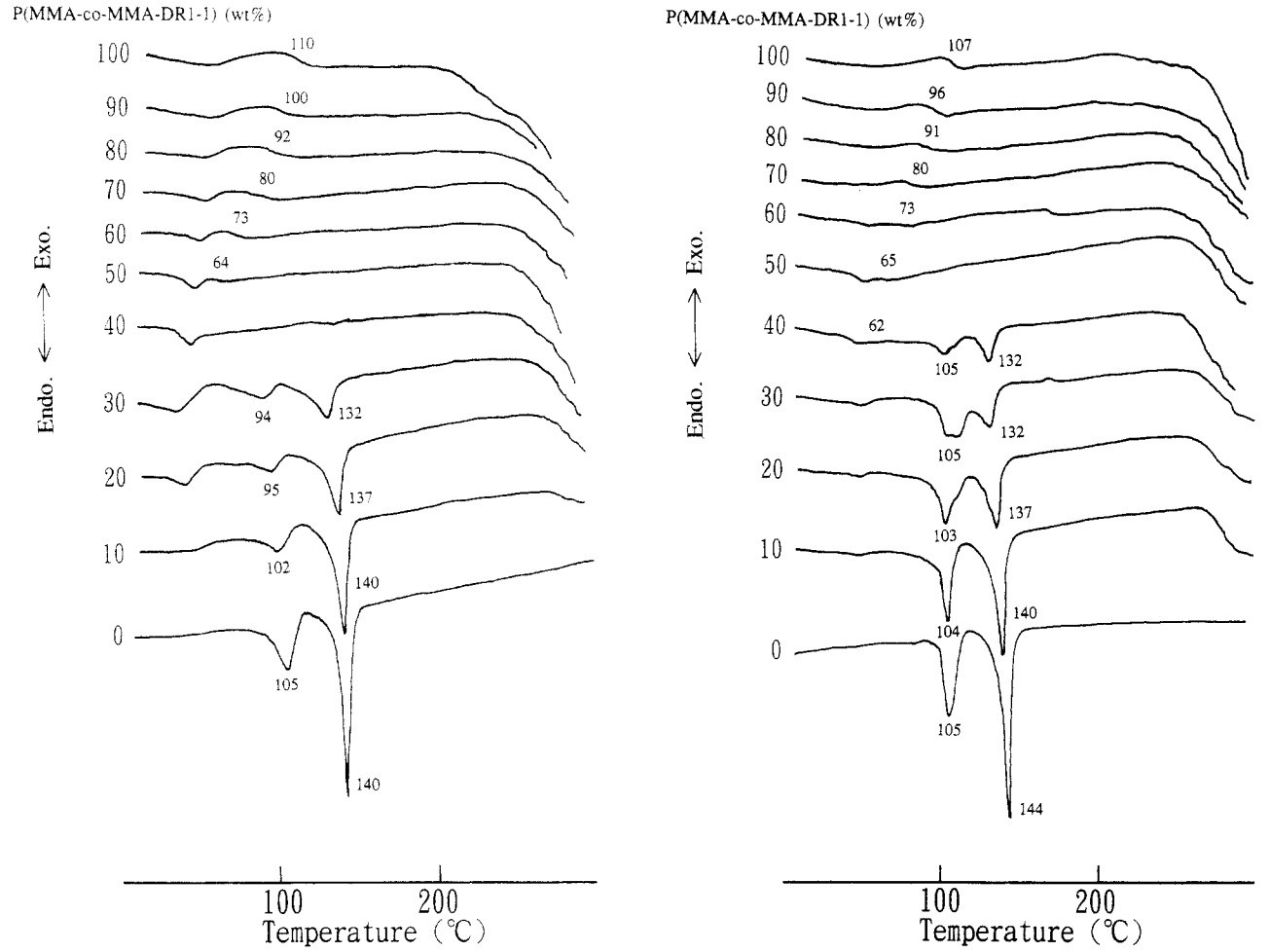

Figure 3. Temperature profiles of DTA scanning of P(VDF-TrFE)/P(MMA-*co*-MMA-DR1-1) for various P(MMA-*co*-MMA-DR1-1) contents at intervals of 10 wt %: (a, left) melt-quenched samples; (b, right) samples annealed at 100 °C for 30 min.

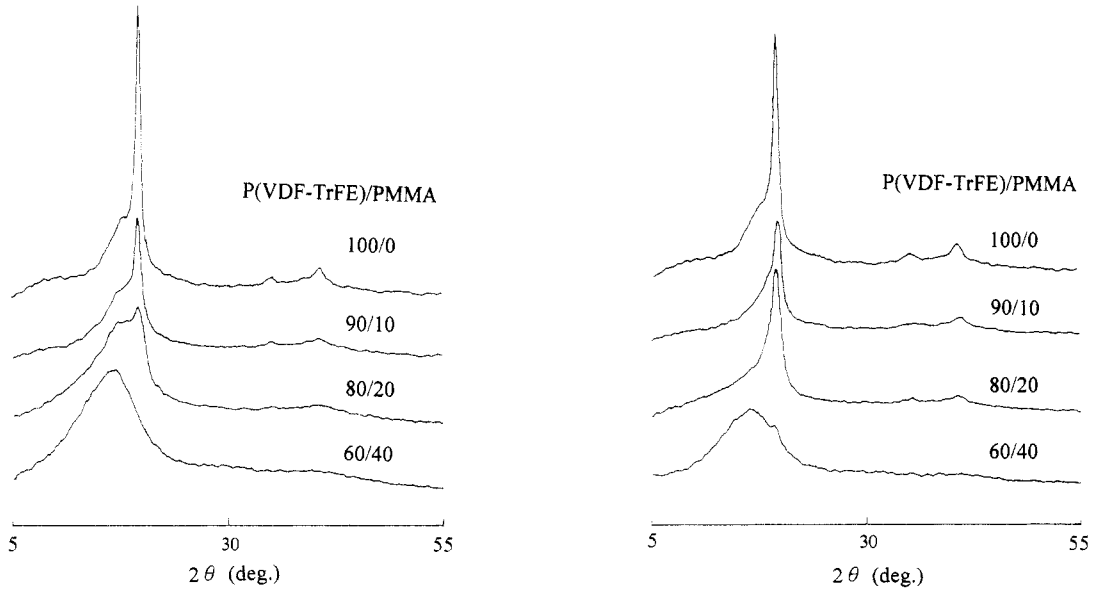

Figure 4. WAXS profiles for melt-quenched P(VDF-TrFE)/PMMA blends (a, left) and for annealed ones at 100 °C for 30 min (b, right).

Obtained crystallite sizes were 55, 50, and 35 Å for (100/0), (90/10), and (80/20) P(VDF-TrFE)/PMMA, respectively. Thus the decrease of β-crystallite size may be responsible for the decrease of E_i and C_{pyro} with decreasing P(VDF-TrFE) content. It is noted that the PMMA neat sample shows an E_i of 1.34 MV/cm, which is higher than the poling field of 0.8 MV/cm. A thermal pulse response showed the existence of space charge due to negative charges. Thus the large E_i in the PMMA neat sample is attributed to this space charge effect.

Thermal Stability of the Internal Electric Field and Pyroelectricity. Parts a–c of Figure 8 show E_i and C_{pyro} of (99/1), (90/10), and (80/20) P(VDF-TrFE)/PMMA samples, respectively. (99/1) P(VDF-TrFE)/PMMA was poled in a Fluorinert at room temperature at a constant field of 1 MV/cm for 1 h, (90/10) and (80/20) P(VDF-

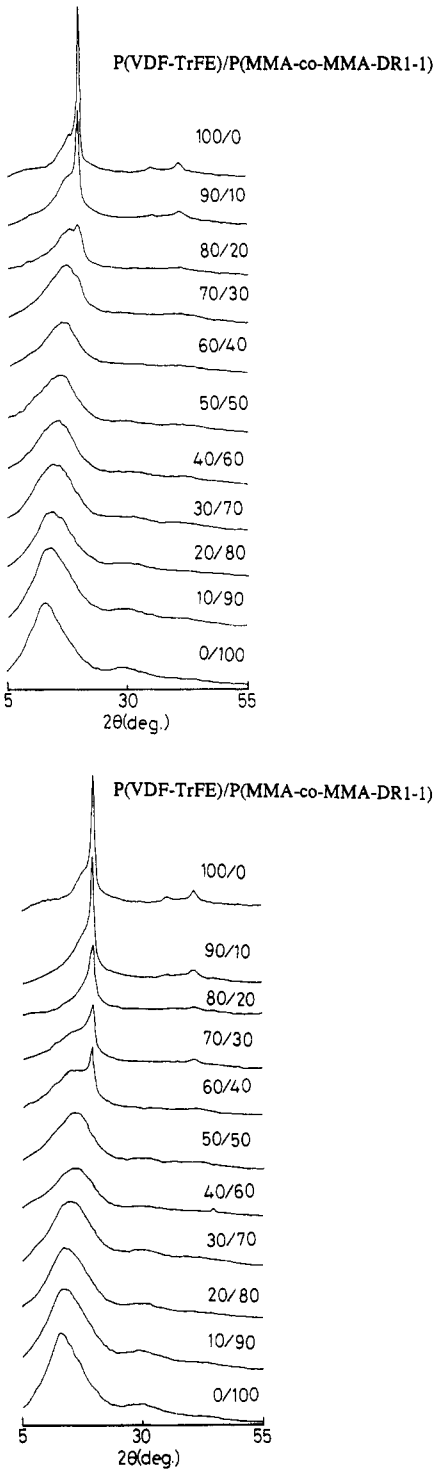

Figure 5. WASX profiles for melt-quenched P(VDF-TrFE)/P(MMA-*co*-MMA-DR1-1) blends (a, top) and for annealed ones at 100 °C for 30 min (b, bottom).

TrFE)/PMMA samples were poled under the same conditions as were used in the case of Figure 7, and then all samples were thermally annealed at successively higher indicated temperatures. After each annealing stage, the sample was returned to ambient temperature for a set of measurements. All the measurements in Figure 8 were made within a few hours of the preceding thermal treatment.

For (99/1) P(VDF-TrFE)/PMMA, significant activity depression of both E_i and C_{pyro} is not measured until the abrupt and complete loss of activity occurs at temperatures between 110 and 130 °C, corresponding to the ferroelectric–paraelectric transition at T_c, measured as 116 °C by DTA for the poled P(VDF-TrFE). The result implies that the

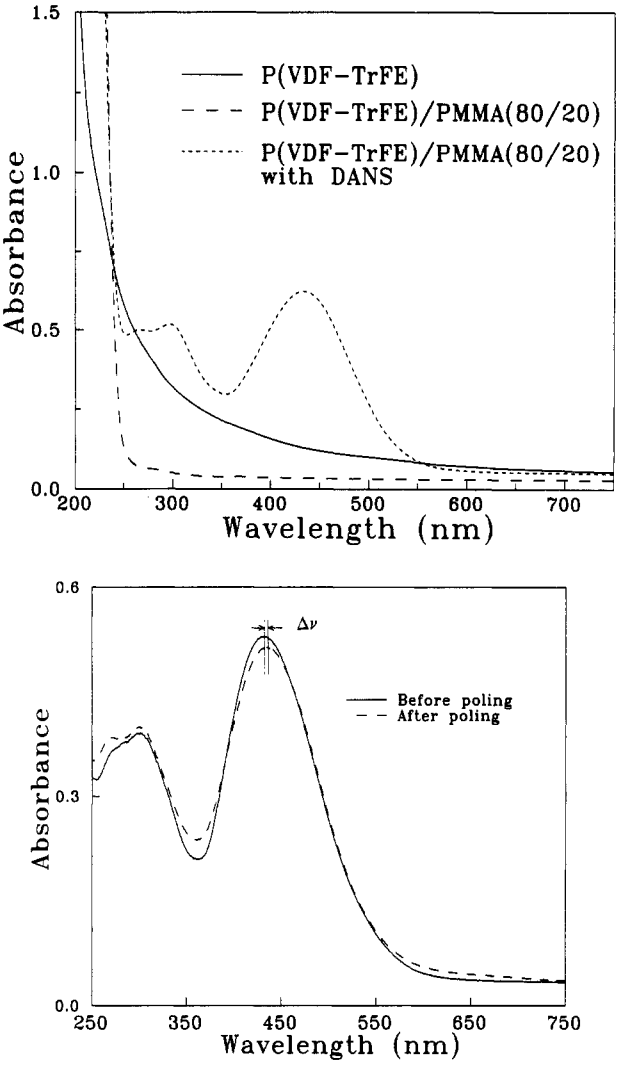

Figure 6. (a, Top) ultraviolet–visible spectra of P(VDF-TrFE), (80/20) P(VDF-TrFE)/PMMA, and DANS containing (80/20) P(VDF-TrFE)/PMMA blends. (b, Bottom) DANS spectra before and after poling.

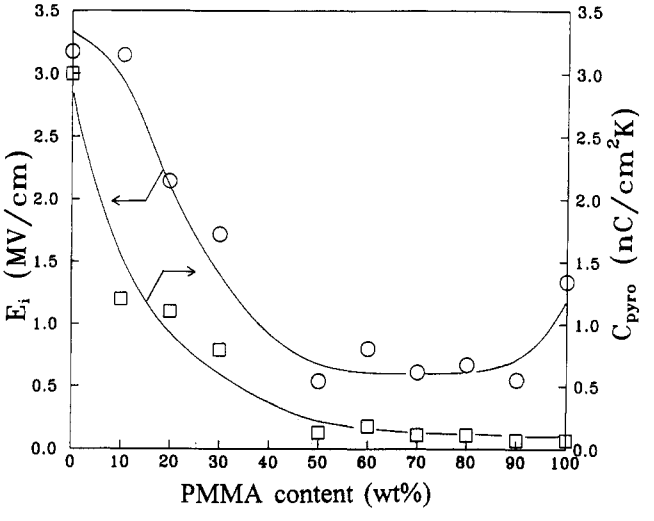

Figure 7. Plots of E_i and C_{pyro} versus PMMA content in P(VDF-TrFE)/PMMA: (○) E_i; (□) C_{pyro}.

significant contribution to E_i and C_{pyro} is from the aligned β-crystallite dipoles. The small increase of E_i is measured in the vicinity of 60 °C. Since the experimental precision of the E_i calculation using eq 9 is within 1% and the experimental scatter between each measurement is also within a few percent, the increase of E_i in the vicinity of 60 °C is not due to the experimental scatter. Tsutsumi

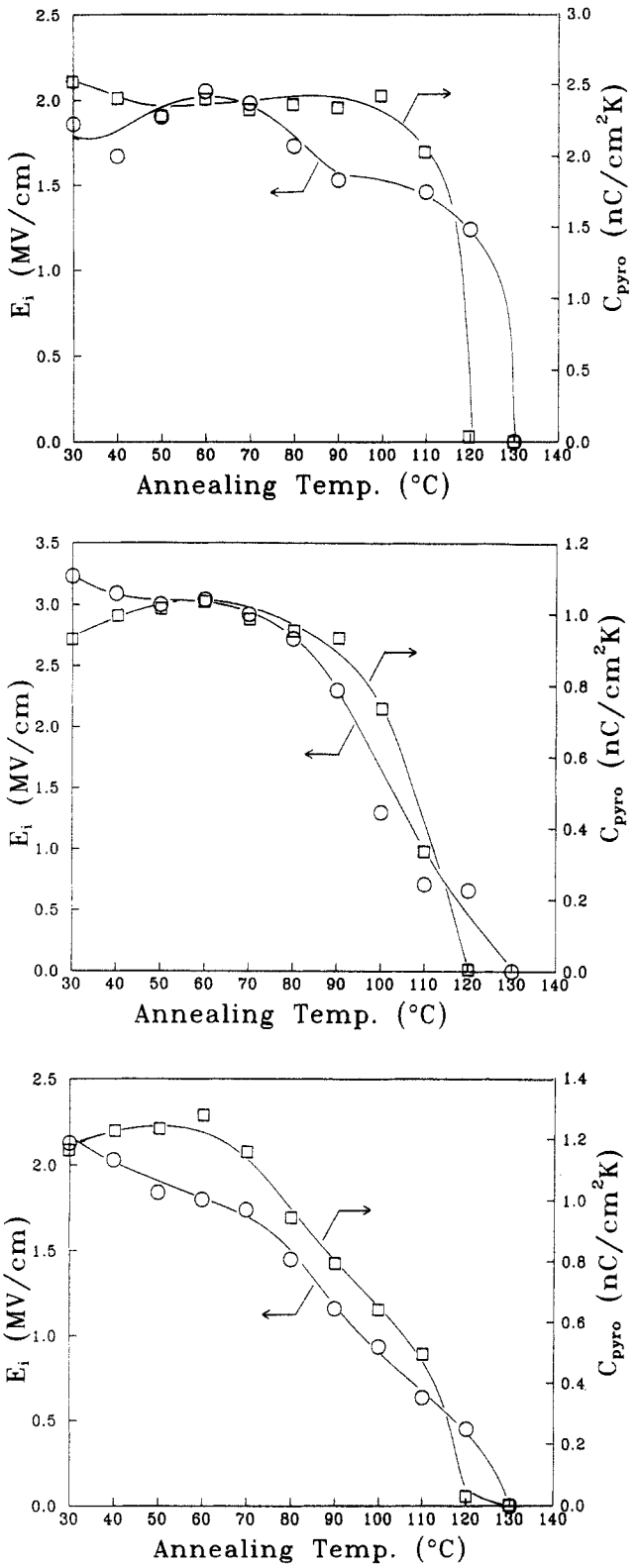

Figure 8. E_i and C_{pyro} after annealing for 30 min at the indicated temperature for (99/1) P(VDF-TrFE)/PMMA (a, top), (90/10) P(VDF-TrFE)/PMMA (b, middle), and (80/20) P(VDF-TrFE)/PMMA (c, bottom): (○) E_i; (□) C_{pyro}.

et al. have already reported that the poling of P(VDF-TrFE) causes the generation of HF, the resultant proton protonating the dyes, and further loss of HF at temperatures above 80 °C.[5,18] They also concluded that such a loss of ionic counter charges at crystal–amorphous interfaces might be responsible for the increase of the internal electric field at temperatures around 80 °C.[5] Thus the present result of a small increase in E_i at temperatures around 60 °C is also due to loss of such a of counter change

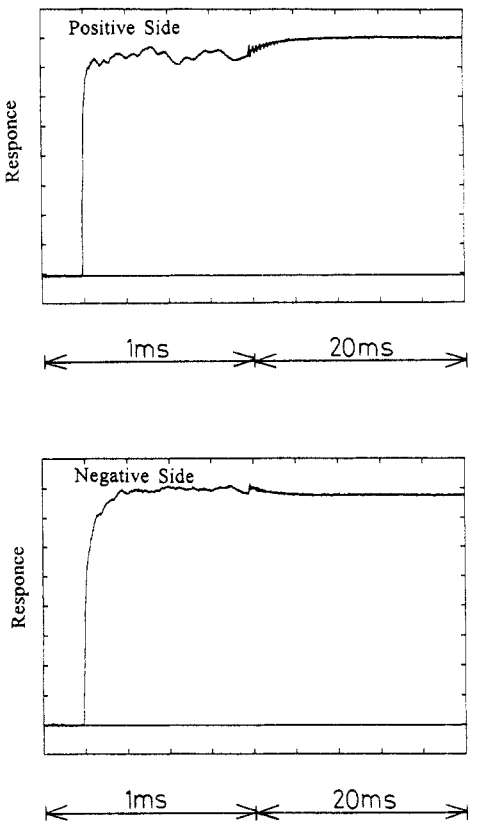

Figure 9. Profiles of polarization and charge distribution in a (80/20) P(VDF-TrFE)/PMMA blend.

(small amount of fluorine ions produced by poling) at crystal–amorphous interfaces.

For (90/10) P(VDF-TrFE)/PMMA, E_i and C_{pyro} are almost constant until their significant activity losses occur at temperatures above 90 °C. (80/20) P(VDF-TrFE)/PMMA has the gradual decrease of E_i at temperatures up to 70 °C followed by the large decrease at temperatures above 70 °C. C_{pyro} is almost constant until the significant decrease occurs at temperatures above 70 °C. These critical temperatures at which large losses of E_i and C_{pyro} start are lower than $T_c \approx 105$ °C but significantly higher than $T_g \approx 39$ and 50 °C measured by TMA for (90/10) and (80/20) blends, respectively. Thus the contribution to E_i and C_{pyro} for (90/10) and (80/20) blends are mainly from β-crystallite dipoles and may be additionally from the amorphous polarization.

Profile of the Polarization Distribution. Figure 9 shows the thermal pulse response for (80/20) P(VDF-TrFE)/PMMA. The sample was poled under the same conditions as used for the case of Figures 7 and 8. The profile of polarization and charge distribution seems to be uniform. Tsutsumi et al.[9] indicated that the (80/20 by weight) PVDF/PMMA blend shows a nonuniform profile of thermal pulse response and a significant decrease of C_{pyro} at temperatures above $T_g \approx 60$ °C. The anomalous stabilization of E_i at temperatures up to 100 °C for PVDF/PMMA was explained by strong space charge effect. However, for the present system of (80/20) P(VDF-TrFE)/PMMA, the thermal stability of E_i corresponds well to that of C_{pyro} shown in Figure 8c; the uniform polarization and charge distribution shown in Figure 9 is given and no space charge effect is observed. The only difference between PVDF/PMMA and P(VDF-TrFE)/PMMA is that PVDF is replaced by P(VDF-TrFE), but it is noted that this difference gives rise to the significant different nature of polarization and charge distribution.

Table I. Refractive Indices (RI) and Coherence Lengths (l_c) for the Samples

sample	RI at 1060 nm	RI at 530 nm	l_c (μm)
P(VDF-TrFE)	1.420	1.453	8.1
P(MMA-co-MMA-DR1-1)	1.498	1.5135	17.2
(90/10) P(VDF-TrFE)/PMMA	1.406	1.427	12.7
(90/10) P(VDF-TrFE)/ P(MMA-co-MMA-DR1-1)	1.427	1.440	20.5

Second Harmonic Generation. A decrease of the refractive index was measured when the wavelength of the probe light was increased for the neat polymer and blend systems studied. Table I shows the refractive indices measured at 530 and 1060 nm and the coherence length calculated from these refractive indices. As shown in Table I, the coherence length is in the range 8–20 μm. Figure 10 shows the typical result of a SHG Maker fringe pattern for (90/10) P(VDF-TrFE)/P(MMA-co-MMA-DR1-1). Since the coherence length is shorter than the film thickness in the range 60–80 μm, the fringer pattern shown in Figure 10 was observed. For (90/10) P(VDF-TrFE)/P(MMA-co-MMA-DR1-4), several trials to measure the refractive indices at both 530 and 1060 nm had been done, but in all cases, no clear line between bright and dark regions in the view of an abbe refractometer could be seen to determine the refractive index, because of the deep red color of the films owing to the larger amount of DR1 dye molecule. Then when the SHG coefficient d_{33} was determined for this blend, the refractive indices and the coherence length for (90/10) P(VDF-TrFE)/P(MMA-co-MMA-DR1-1) were used.

An SHG coefficient d_{33} of 3.3×10^{-9} esu was measured for P(VDF-TrFE) poled at 1 MV/cm for 1 h in a Fluorinert. Hill et al. have already reported the d_{33} value of $(4.1 \pm 2) \times 10^{-10}$ esu for the corona poled P(VDF-TrFE) copolymer with E_i = 1.1 MV/cm.[19] In the theoretical expression of the SHG, coefficient d_{33}[19,20] can be written as

$$d_{33} = \frac{N f_\omega^2 f_{2\omega} \beta \mu_g E_i}{10kT} \tag{18}$$

where N is the number density of noncentrosymmetric dipoles or the NLO guest pendant moiety, β is the hyperpolarizability of the dipole or NLO guest, and f_ω and $f_{2\omega}$ are Lorentz–Lorentz local field factors. From this expression, the SHG coefficient could be linear with E_i. Thus the large value of d_{33} in this study may be due mainly to the large E_i of 3–4 MV/cm.

SHG coefficients d_{33} for P(VDF-TrFE) and (90/10) P(VDF-TrFE)/PMMA samples measured at successively higher temperatures are plotted against the temperatures in Figure 11a,b, respectively. The (90/10) P(VDF-TrFE)/PMMA sample was poled under the same conditions as used for the case of Figure 7. For P(VDF-TrFE), the significant activity loss of d_{33} is not measured until its abrupt decrease occurs at the temperatures above 110 °C, corresponding to $T_c \approx 116$ °C for the poled P(VDF-TrFE). The small increase of d_{33} measured in the vicinity of 70 °C may be related to the small increase of E_i around 60 °C shown in Figure 8a due to the loss of ionic counter charge (small amount of fluorine ions produced by poling) at the crystallite–amorphous interface.

For (90/10) P(VDF-TrFE)/PMMA, the gradual decrease of d_{33} at the temperatures between 40 and 60 °C is due to the molecular relaxation of the amorphous dipoles around the glass transition region ($T_g \approx 39$ °C for TMA measurement). This temperature profile of d_{33} corresponds well to that of E_i shown in Figure 8b. This similarity

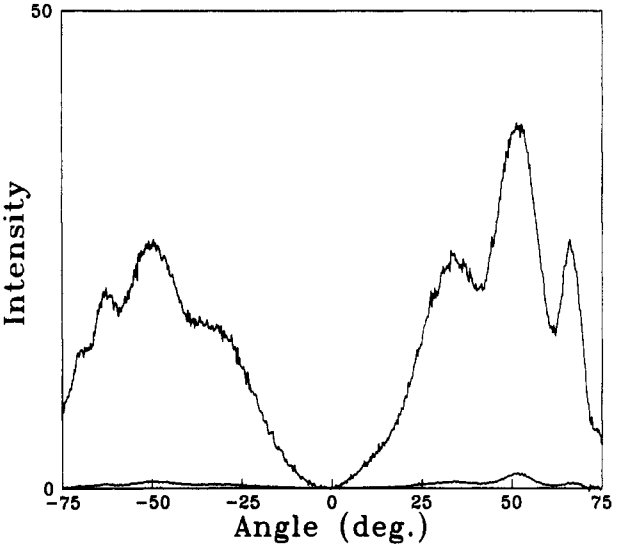

Figure 10. SHG Maker fringe pattern of (90/10) P(VDF-TrFE)/P(MMA-co-MMA-DR1-1).

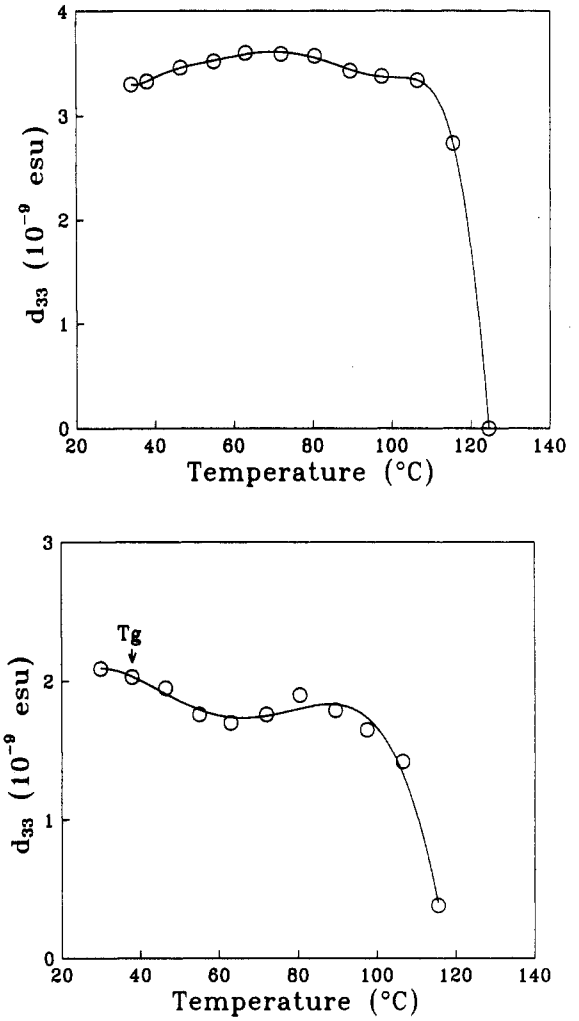

Figure 11. Temperature dependence of SHG coefficient d_{33} for P(VDF-TrFE) (a, top) and for a (90/10) P(VDF-TrFE)/PMMA blend (b, bottom).

should be natural, because the nature of thermal stability of both E_i and d_{33} is attributed to the aligned β-crystallite dipoles.

Figure 12 shows the temperature profile of d_{33} for (90/10) P(VDF-TrFE)/P(MMA-co-MMA-DR1-4). The P(VDF-TrFE)/P(MMA-co-MMA-DR1-4) sample was poled at 0.8 MV/cm at 100 °C for 30 min and cooled to

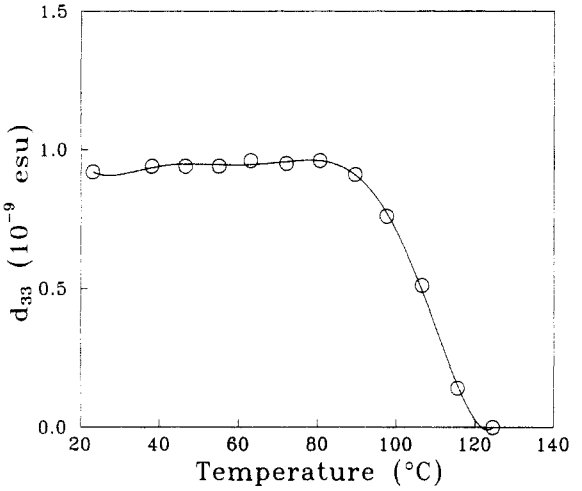

Figure 12. Temperature dependence of SHG coefficient d_{33} for (90/10) P(VDF-TrFE)/P(MMA-*co*-MMA-DR1).

room temperature for 30 min under the same field prior to SHG measurement. The conditions of measuring the SHG are the same as used for P(VDF-TrFE) or P(VDF-TrFE)/PMMA in Figure 11. As shown in Figure 12, no significant decrease of d_{33} is measured until its large decrease occurs at temperatures above 90 °C, which corresponds well to the d_{33}–temperature profile for (90/10) P(VDF-TrFE)/PMMA in Figure 11b. It is particularly important to note that d_{33} for the P(VDF-TrFE)/P(MMA-*co*-MMA-DR1-4) blend is thermally stable at T_g (may be close to 39 °C) because the main contribution to SHG activity is due to the aligned β-crystallite dipoles and NLO dyes noncentrosymmetrically oriented by E_i whose molecular relaxation essentially occurs in the vicinity of the Curie temperature which is higher than T_g. An attempt to make the optically transparent and clear blend of P(VDF-TrFE) with P(MMA-*co*-MMA-DR1-8) and that with P(MMA-*co*-MMA-DR1-14) failed because of the phase separation in the amorphous region of P(VDF-TrFE)/P(MMA-*co*-MMA-DR1) with high DR1 content.

Conclusion

We have found that the poling-induced internal electric field in the P(VDF-TrFE)/PMMA blend whose P(VDF-TrFE) content is above 70 wt % is greater than the applied field, as is the case for another ferroelectric host.[5,8,9] P(VDF-TrFE)/PMMA and P(VDF-TrFE)/P(MMA-*co*-MMA-DR1) with low DR1 contents (experimentally up to 4 mol %) have optical clarity from the near infrared to ultraviolet regions of spectrum, even if they have a β-crystallite phase. This may be due to the depression of the growth of spherulite in the blends. E_i, C_{pyro}, and d_{33} are stable until their abrupt decrease occurs when one approaches the Curie transition temperature. It is noted that these blends are not subject to the significant activity loss of E_i, C_{pyro}, and d_{33} at the glass transition temperature, which is usually responsible for the molecular relaxation of aligned dipoles and NLO molecules in the amorphous phase of nonferroelectric polymeric materials. These desirable properties qualify the ferroelectric blends to be a new candidate for SHG materials.

Acknowledgment. We gratefully acknowledge Dr. G. Thomas Davis, Polymer Division, National Institute of Standards & Technology, for helpful discussion and Dr. Aime S. DeReggi for the cooperative measurement of the polarization distribution by the thermal pulse method and numerous discussion. This work is supported in part by Grants-in-Aid for Scientific Research, No. 04650810, and for International Scientific Research, Joint Research No. 03044090, from the Ministry of Education, Science, and Culture, Japan.

References and Notes

(1) Eich, M.; Sen, A.; Looser, H.; Bjorklund, G. C.; Swalen, J. D.; Twieg, R.; Yoon, D. Y. *J. Appl. Phys.* **1989**, *66*, 2559.
(2) Eich, M.; Reck, B.; Yoon, D. Y.; Willson, G. C.; Bjorklund, G. C. *J. Appl. Phys.* **1989**, *66*, 3241.
(3) Papers presented in: *Organic Materials for Non-linear Optics II*; Hann, R. A., Bloor, D., Eds.; The Royal Society of Chemistry: Cambridge, U.K., 1991.
(4) Hill, J. R.; Pantelis, P.; Davis, G. J. *Ferroelectrics* **1987**, *76*, 435.
(5) Tsutsumi, N.; Davis, G. T.; DeReggi, A. S. *Macromolecules* **1991**, *24*, 6392.
(6) Saito, K.; Tasaka, S.; Miyata, S.; Jo, Y. S.; Chujo, R. *Nippon Kaggaishi* **1985**, 1909.
(7) Nishi, T.; Wang, T. T. *Macromolecules* **1975**, *8*, 909.
(8) Tsutsumi, N.; Ueda, Y.; Kiyotsukuri, T. *Polymer* **1992**, *33*, 3305.
(9) Tsutsumi, N.; Ueda, Y.; Kiyotsurkuri, T.; DeReggi, A. S.; Davis, G. T. *J. Appl. Phys.*, in press.
(10) Maker, P. D.; Terhune, R. W.; Nisenoff, M.; Savage, C. M. *Phys. Rev. Lett.* **1962**, *8*, 21.
(11) Jerphagnon, J.; Kurtz, S. K. *J. Appl. Phys.* **1970**, *40*, 1667.
(12) Mopsik, F. I.; DeReggi, A. S. *J. Appl. Phys.* **1982**, *53*, 4333.
(13) DeReggi, A. S.; Broadhurst, M. G. *Ferroelectrics* **1987**, *73*, 351.
(14) Liptay, W. In *Excited States*; Lim, E. C., Ed.; Academic Press: New York and London, 1974; Vol. I, pp 129–229.
(15) Havinga, E. E.; van Pelt, P. *Ber. Bunsen-Ges. Phys. Chem.* **1979**, *83*, 816.
(16) Prasad, P. N.; Williams, D. J. In *Introduction to Nonlinear Optical Effects in Molecules & Polymers*; Prasad, P. N., Williams, D. J., Eds.; Wiley-Interscience: New York, 1991; Chapter 6.
(17) Tajitsu, Y.; Ogura, H.; Chiba, A.; Furukawa, T. *Jpn. J. Appl. Phys.* **1987**, *26*, 554.
(18) Tsutsumi, N.; Davis, G. T.; DeReggi, A. S. *Polym. Commun.* **1991**, *32*, 113.
(19) Pantelis, P.; Hill, J. R.; Davies, G. J. In *Nonlinear Optical and Electroactive Polymers*; Prasad, P. N., Ulrich, D. R., Eds.; Plenum Press: New York, 1988; pp 229–241.
(20) Prasad, P. N.; Williams, D. J. In *Introduction to Nonlinear Optical Effects in Molecules & Polymers*; Prasad, P. N., Williams, D. J., Eds.; Wiley-Interscience: New York, 1991; Chapter 4, pp 66–73.